A Comparative Analysis of Power Converter Topologies for Integration of Modular Batteries in Electric Vehicles

Alberto Cárcamo[1], Aitor Vázquez[1], Alberto Rodríguez[1], Diego G. Lamar[1], Marta M. Hernando[1], Daniel Remón[2]
University of Oviedo, E+ Ecoeficiencia e Ingeniería S.L. [2]
Edificios Departamentales Oeste, Mod. 3, 33204, C. Gregorio Marañón, 1, 33203
Gijón, España
uo278796@uniovi.es

Acknowledgements

This work has been supported by the Principality of Asturias and FICYT under project SV-PA-21-AYUD/2021/51931 and by the Spanish Government under project PID2021-127707OB-C21.

Keywords

«Bi-directional converters», «Dual Active Bridge (DAB) DC-DC converter», «Battery charger», «Power converters for EV».

Abstract

This paper presents a comparative analysis between four proposed DC-DC power converter topologies, for integration of removable batteries into an electric vehicle (EV) that also has a primary energy storage system (ESS). To perform this analysis, first the minimum requirements for the converter are defined, such as volume, power density, and specific density, as well as the system operating condition. The comparison between the proposed topologies is done by evaluating three main aspects: efficiency, volume, and current ripples. The procedure consists of performing a steady-state analysis of each topology to obtain the main operating values and waveforms, validating the results and the proposed control strategies through simulations, calculating the losses for each converter, and estimating their volume. Different components are evaluated in each topology to perform a power loss analysis, considering several options of Si MOSFETs, transformers, and inductors.

Introduction

EVs are becoming a trend in the past years and are foreseen to dominate the future in mobility [1], as new technologies are developed, and prices become competitive in comparison with the Internal Combustion Engine Vehicles (ICE). The commitment of the world with reducing the carbon emissions has contributed to the increase of research and development of EV systems, including the power converter topologies, whose research is oriented at increasing efficiency, reliability, as well as the reduction of their size and weight [2]. All this is supported with the governments' policies which are being updated in order to support this technology, especially in the European Union (EU) [3].

EVs usually has only one ESS, typically a non-removable battery. There have been several proposals regarding EV designs, which consider implementing a primary removable battery, which can be replaced by technicians, rather than the user, using specialized equipment. This is not only due to safety reasons but also due to the size and weight of the battery [4]. The impact on the electrical grid may also be addressed, by charging the batteries at off-peak periods, or even providing grid support [5]–[7], while including the possibility of extending the batteries life by charging them in slow-charging mode [8]. Battery swapping has been offered in 2013 by different companies, but failed due to lack of interest from customers or cooperation from manufacturers [9] [10]. Among the different proposals, this paper studies a system that considers the use of modular removable batteries in addition to a main non-

removable battery. These additional batteries can be considered as a secondary ESS for the EV, which allows an increased flexibility of the energy management, and the possibility of increasing the EV range, among other things. Fig. 1 shows the power system that is considered for this study. It comprises a primary non-removable battery connected to the HV-DC bus through a BMS, which is always mandatory as it provides functions such as balancing the charge of the cells [11], monitoring the temperature, providing safety measures, among other functions. The HV-DC bus supplies power to the LV-DC bus, where the electronic control units (ECUs) and the auxiliary electronic systems are. It also supplies power to the electric motors through the inverters. The system has an additional EES connected to the HV-DC bus, the secondary removable batteries, which are integrated by connecting them through a BMS and a power converter, the latter being the converter under analysis in this paper.

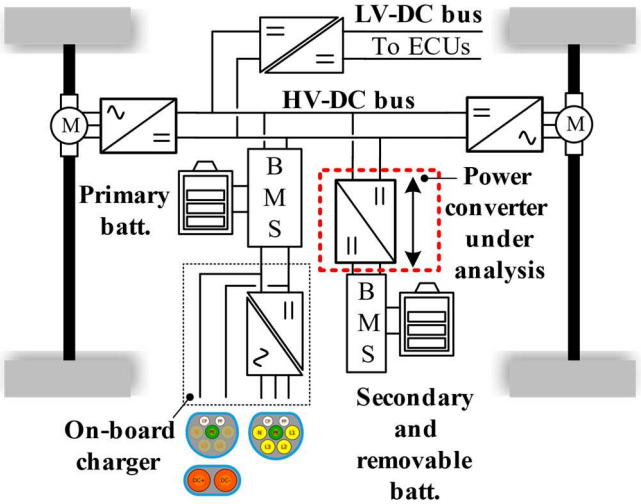

Fig. 1: EV power system, with a main non-removable battery and secondary removable batteries, connected through a converter (red dotted).

The converter should be able to work on a system with certain characteristics and comply with the requirements defined below. One of the characteristics of the system is the range of voltage variations in the secondary batteries (input port), and in the HV-DC bus (output port). This voltage range depends on the State of Charge (SoC) of the removable batteries at the input port, and the HV-DC voltage at the output port, which is set by the primary battery at a nominal voltage that can vary from 200V to 450V [12]. Due to these voltage variations, the converter design should be able to operate in a relatively wide range of voltages in the input and output [13]. The converter should also be bidirectional, to sink energy from the HV-DC bus, either for regenerative breaking, or to allow the charging of the secondary batteries directly from the HV-DC bus, without removing them from the vehicle. The requirements defined for this study are shown in Fig. 2 and are as follows: nominal power of 10 kW, nominal voltage of 60V and 400V for the input and output, respectively, a volume of 4.6 dm^3 specified by the maximum dimensions of 575 x 100 x 80 mm and a maximum weight of 10 kg, which gives a resultant minimum power density of 2.174 kW/ dm^3 and a specific density of 1 kW/kg.

Four topologies are chosen for this comparative analysis. Two of them are based on a boost converter: the Input-Parallel Output-Parallel boost converter (IPOP), and the Cascaded-Boost converter (CB). The other two topologies are based on a phase-shifted full-bridge converter providing galvanic isolation through a transformer: Current-Fed Phase-Shifted Full-Bridge converter (CF-PS-FB), and the Dual-Active-Bridge converter (DAB).

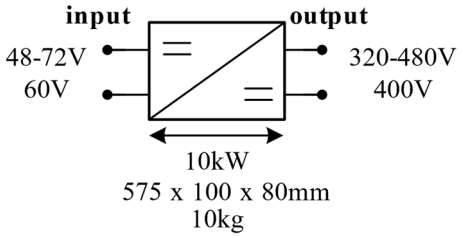

Fig. 2: Converter design requirements and system specifications.

The paper is organized as follows: the proposed topologies are described in Section II, Section III shows the methodology used for the comparison, the results of the analysis are summarized in Section IV, and finally the conclusions are presented in Section V.

Proposed Power Converter Topologies

Input-Parallel Output-Parallel Converter (IPOP)

The IPOP converter is a modular Boost Converter with three modules connected in parallel at the input and at the output, as can be seen in Fig. 3 [14]. Each module of the converter handles one third of the total power, allowing the use of components with lower current rating. The control signals of each module are 120° phase-shifted to reduce the current ripple at the input.

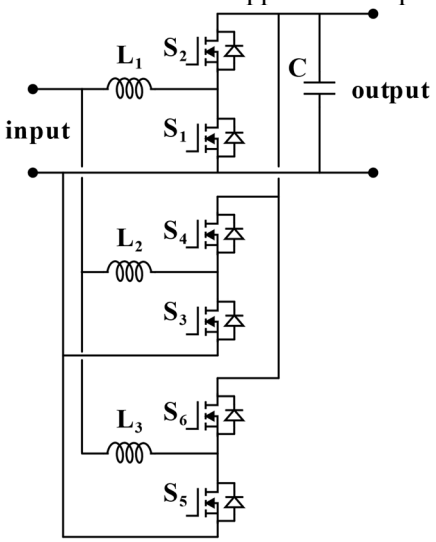

Fig. 3: IPOP converter schematic.

Due to the large voltage ratio between the input and output, it is necessary to work at a high nominal duty cycle in each module, around 85%. This causes the grounded MOSFET power transistors (S1, S3 and S5) to conduct a larger current than the floating ones (S2, S4 and S6). Therefore, the conduction losses in these devices are unbalanced, and entails the selection of their model to be carried out independently for the grounded and for the floating devices. This is further explained in Section III.

This topology has two advantages: the reduction of the current rating of the power transistors and the decrease of the current ripple at the input. These advantages are a consequence of the modular arrangement and the interleaved control. Among the disadvantages, it can be mentioned the high duty cycle and the asymmetry, the increased volume due to the inductors of each module, and the operation with hard switching of the MOSFETs, which lowers its efficiency, specially at high switching frequencies.

Cascaded-Boost Converter (CB)

The CB converter, which is also based on a modular boost converter, is made up of 2 stages that are cascaded through a DC bus [15]. Fig. 4 shows the CB converter schematic. The first stage, which is connected to the input, is a two-module IPOP boost converter that works with a fixed 50% duty cycle and with an interleaved control that is phase-shifted 180° to reduce the current ripple, virtually eliminating it completely. The fixed duty cycle boosts the input voltage to double its value, resulting in a nominal voltage at the DC bus of 120 V. The second stage is a boost converter, which boosts the DC bus voltage to the HV-DC bus voltage (400 V).

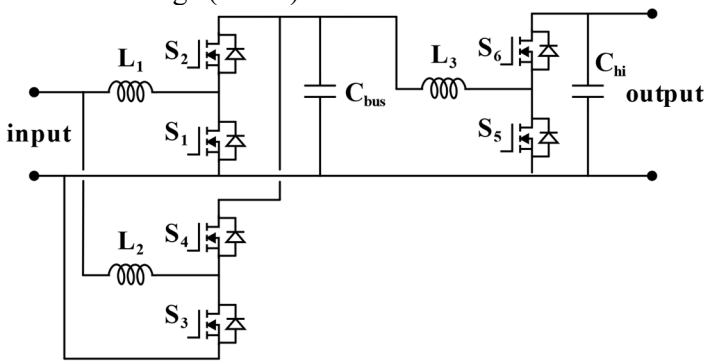

Fig. 4: CB converter schematic.

Besides virtually cancelling all the current ripple at the input, another advantage of working at a 50% duty cycle is that the MOSFETs used in the first stage have the same current flowing through them, making it possible to select the same model for the ground-referenced and the floating-referenced device. The voltage at the DC-bus allows the use of low voltage rated devices in the first stage, while using high voltage rated devices on the second stage. At the second stage, the MOSFET selection may be done independently, although its nominal duty cycle is not as high as in the IPOP, it is around 75%.

An independent control strategy is proposed for each stage. The first stage has a cascaded control with the outer loop controlling the voltage at the DC-bus, and a current controller at the inner loop that regulates and balances the currents in each module. The second stage has a current controller, which receives the reference of the power flow, regulating the dynamic behavior of the converter.

One disadvantage identified on this topology is the volume, as it needs an extra capacitor for the DC-bus, and besides the two inductors of the first stage, it needs an inductor at the second stage that is rated for the full 10 kW of power. The control is also more complex than the one for the IPOP.

Current-Fed Phase-Shifted Full-Bridge Converter (CF-PS-FB)

The CF-PS-FB converter is the first proposed topology that offers galvanic isolation, and it is based on two Full-Bridges (FBs), a current-fed FB at the input and a voltage-fed FB at the output. The input FB is connected to the secondary batteries through an inductor, and has an active clamp made from a transistor and a capacitor for achieving soft-switching [16]. Both FBs are connected through a transformer, and optionally an inductor can be added in series. Fig. 5 shows its schematic.

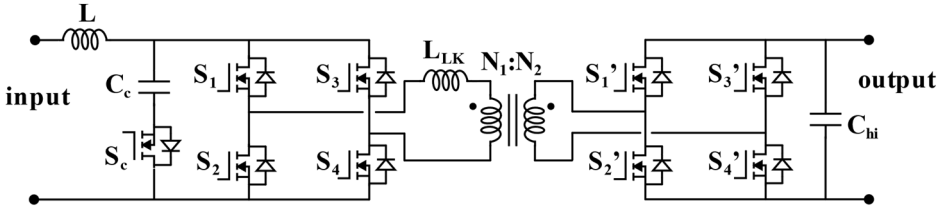

Fig. 5: CF-PS-FB schematic.

This converter has two operating modes depending on the direction of the power flow: boost mode (input to output) and buck mode (output to input). In boost mode, the input FB operates as a current-fed FB converter, while the output FB works as a synchronous rectifier. In buck mode, the output FB operates as a voltage-fed converter while the input FB operating as a synchronous rectifier. The active clamp allows the possibility of the converter to operate under Zero-Voltage Switching (ZVS) and Zero-Current Switching (ZCS) [17].

One disadvantage of this converter is the need of changing the operating mode when the direction of the power flow changes, which besides increasing the complexity of the control, it also takes some time, which can limit the dynamic response of the converter. Also, this converter has more components, including an additional circuit for demagnetizing the input inductor at the turning on of the converter, as well as in case of failure. This extra circuitry is not shown in Fig. 5.

Dual Active Bridge Converter (DAB)

The DAB is also based on two FBs, connected through a transformer, using an inductance to transfer power, naturally behaving as a current source. Usually, this inductance is added as an external inductor, however, the transformer leakage inductance may also be used. The DAB converter schematic is shown in Fig. 6. Although the power transfer in this topology depends on several factors, it is important to note that given a previously defined and fixed switching frequency, the value of the inductance, L_{LK}, is the one that defines the maximum power the converter is capable of transferring, being this inductance inversely proportional to the power.

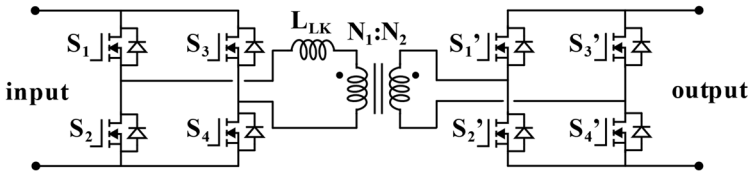

Fig. 6: DAB converter schematic.

There are several control techniques [18] [19], but the simplest and the one considered for this study is the Single Phase-Shift (SPS) control. This technique consists in using a fixed duty cycle of 50% in both FBs, and introducing a phase-shift between them, which is the control variable for the power flow.

One of the advantages of this topology is the ZVS operation, which allows to transfer relatively high power with high efficiency. Note that ZVS is not always guaranteed, as it is lost when operating at low power, or at wide range of voltages [20]. However, there are several solutions to extend the ZVS operation point, even throughout all range of power transfer, and a wide voltage range. Some solutions include the use of more complex control strategies, such as Triple Phase-Shift (TPS), or using the transformer magnetizing inductance to increase the reactive current [21]. Considering SPS control, the design approach followed is oriented to maximize its efficiency at a certain power, although this implies reducing the efficiency at other operating points. The disadvantage of this converter is mainly the high current ripple.

Methodology

Analysis Parameters

To perform the analysis between the proposed topologies, the following parameters are evaluated:

- Current Ripple: The peak-to-peak value of the current ripple, at both the input and the output, is evaluated. Topologies with high current ripples may require the addition of external filters, which will add volume and weight to the final design. It is important to mention that these filters are not included in this analysis.

- Efficiency: An estimation of the transistor power losses is carried out. The magnetic elements efficiency performance is also evaluated through simulation. Losses due to gate drivers, control circuits, or capacitors series resistance are not considered in this analysis.
- Volume: For the volume estimation, only the magnetic elements (inductors and transformers) are considered. Heat dissipation is done by employing the chassis as heatsink, hence, no additional heat sink is considered. The volume of the capacitors is also neglected.

Analysis Procedure

The procedure for the comparative analysis is summarized as follows:

Steady-State Analysis and Simulation

A steady-state analysis is performed on each of the proposed topologies to obtain the theoretical operating values, which includes the current ripples, the average and rms currents, peak values, among other. This analysis is performed at the nominal power of 10 kW and nominal input and output voltages of 60 and 400 V, respectively. It is important to note that for this analysis, four different frequencies are evaluated on each topology: 25, 50, 75, and 100 kHz.

The result from the steady-state analysis is then validated by comparing them to the simulation results, using the software PSIM® and SIMULINK®. The simulations are also used to validate the control strategies exposed in Section II.

Component Selection

The component selection is a crucial part of this analysis as the converter performance is directly related to their characteristics. This analysis is carried out for the switching devices (MOSFETs), and the magnetic elements (inductors and transformers). Regarding the selection of the switching devices, several part numbers are evaluated for each topology, selecting the ones that provide the best efficiency for the converter. The MOSFETs are divided in two groups: high voltage and low voltage devices. The former are super-junction MOSFETs with a maximum rated break-down voltage of 600-650 V, while the latter are MOSFETs with a maximum break-down voltage of 100-200 V. As mentioned earlier in the paper, there are cases in which the devices are evaluated independently, e.g., the same half-bridge might have 2 different part numbers. For the IPOP, the ground referenced MOSFETs are evaluated independently from the floating-referenced ones, with all of them being high voltage devices. For the CB, the first stage devices are all the same, while in the second stage, the devices are evaluated independently. Also, the first stage considers only low voltage devices, while high voltage devices are considered for the second stage. For the CF-PS-FB and the DAB, the high voltage devices are evaluated on the input FB and the high voltage devices at the output FB, where in both topologies there are no independent evaluations performed. All the devices are rated for automotive applications, and only Silicon (Si) MOSFETs are considered, excluding technologies such as Silicon Carbide (SiC) and Gallium Nitride (GaN), due to their higher cost. Another aspect taken into consideration is the parallelization of the MOSFETs, as it allows the inclusion of devices with good characteristics, but that do not comply with the current rating requirements.

Regarding the magnetic elements, design tools Magnetics Inductor Designer® and Ansys PExprt® are used for the design, selection, and losses estimation for the inductors, while the transformers are selected from commercial options.

Power Losses Analysis

This analysis is divided in two parts: the power losses due to the switching devices, and the power losses in the magnetic components. Regarding the losses on the MOSFETs, only the conduction and switching losses are considered, neglecting the losses due to the gate drivers and the body diode reverse recovery, among others. Although there are several models for calculating the MOSFET switching losses, some

of them very precise and complex, a simplified model is used, defined by equation (1), where, P_{sw} are the switching losses, f_{sw} is the switching frequency, and E_{on} and E_{off} are the turn-on and turn-off losses, respectively. Equation (2) is an expansion of equation (1), where V_{DS} and i_{DS} are the drain to source voltage and the drain current, respectively. $t_{on/off}$ is the time it takes the MOSFET to turn-on/turn-off, and is usually given by the manufacturer [22].

$$P_{sw} = f_{sw}\left(E_{on} + E_{off}\right) \tag{1}$$

$$E_{on/off} = \frac{1}{2} \cdot V_{DS} \cdot i_{DS} \cdot t_{on/off} \tag{2}$$

Note that for the CF-PS-FB and the DAB topologies, because they work with soft-switching, the turn-on losses are neglected and only the turn-off losses are considered. Regarding the magnetic elements, the inductor losses are estimated through the simulations, while the transformer losses are estimated using their datasheet.

Volume Estimation

To estimate the volume of the magnetic components, design tools are used for estimating the volume of the inductors while the transformer dimensions are obtained from the datasheet, as it is a commercial device. In the next section, a more detailed analysis is presented regarding the inductors, as well as the transformers.

Results

Current Ripple

The current ripple value at the input and output for each converter is presented in Table I. The IPOP and CB presents the lowest input current ripple, due to the interleaving, with the CB presenting the best results. However, both topologies present a high output current ripple, with the CF-PS-FB converter presenting the most balanced results at the input and output, with 34.48 and 37 A, respectively. The DAB presents the highest current ripple, both at the input and at the output, due to the reactive current, a characteristic of this topology that is necessary to achieve ZVS.

Table I: Peak-to-Peak Current Ripple

	IPOP	CB	CF-PS-FB	DAB
Input Current Ripple [A]	5.8	0.4	34.48	523.77
Output Current Ripple [A]	60.12	80.84	37.36	244.72

Efficiency

The efficiency results mainly depend on the component selection and the switching frequency at which the converter operates. Table II shows the selected components (part number) for each converter, as they exhibited the best efficiency results for their respective topology. This table also shows the number of parallelized MOSFETs and distinguishes the ones that are evaluated independently. Table III shows the selected magnetic components for each topology in function of the switching frequency. It also shows the core material and part number for the inductors (L1, L2, and L3), and the type and part number for the transformer (T1), which is a 15 kW planar transformer from HIMAG PLANAR® for all frequencies.

Fig. 7 shows a comparison of the power losses and efficiency between the four topologies, where the power losses on the switching devices are shown in Fig. 7(a), the power losses on the magnetic elements

are shown in Fig. 7(b), and the total efficiency is shown in Fig. 7(c). As expected, in Fig. 7(a), the MOSFET power loss increase as frequency increases, as the switching losses are directly proportional to the frequency. However, they increase with a steeper slope on the IPOP and CB topologies, due to hard switching. For the CB, the magnetic losses are reduced at higher frequencies, and for frequencies above 75 kHz, it has the best results after the IPOP. Note that in Table III, the inductor's core material changes according to the switching frequency, however, this does not necessarily imply the reduction of the losses as frequency increases, as it is seen for the DAB in Fig. 7(b), where losses increase from 50 kHz to 75 kHz. A deeper analysis should be performed to understand this behavior, as it is out of the scope of this paper. Regarding the total efficiency, which is shown in Fig. 7(c), the DAB presents the best results, followed by the CF-PS-FB. This is due to their ability to operate at ZVS condition, noting that at 25 kHz, the difference between the four topologies is very small, presenting an efficiency of 93.92%, 94.74%, 94.89% and 96.51 %, for the IPOP, CB, CF-PS-FB, and DAB, respectively.

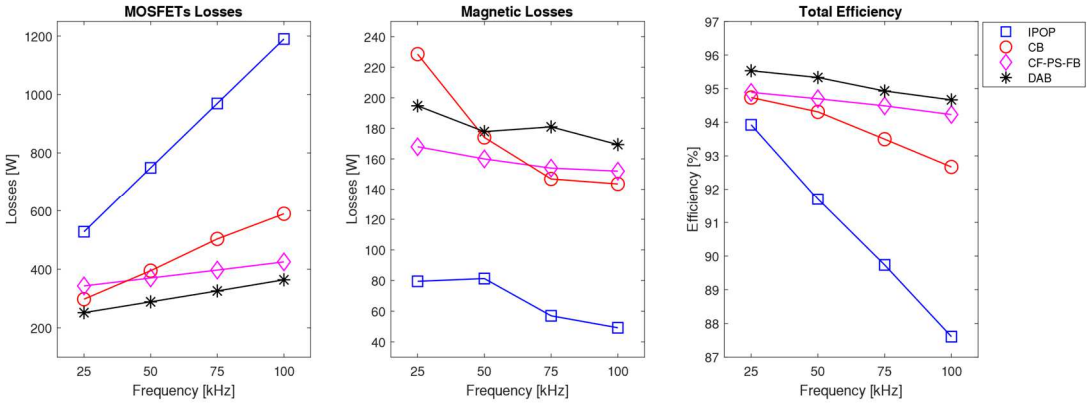

(a) (b) (c)

Fig. 7: Comparative analysis between the proposed topologies: IPOP (blue), CB (red), CF-PH-FB (magenta), and DAB (black), evaluated in function of the switching frequency. (a) MOSFET Losses, (b) Magnetic Losses, (c) Total Efficiency.

Table II: Component Selection (MOSFETs)

	MOSFET		Parallel MOSFETs
IPOP	**Ground-referenced**	STW68N65DM6-4AG	2
	Floating-referenced	IPB65R099CFD7A	1
CB	**1st Stage**	IRF7779L2TRPBF	1
	2nd Stage	IPB65R099CFD7A	5
CF-PS-FB	**Input**	NVHL082N65S3F	1
	Output	IPB044N15N5ATMA1	1
DAB	**Input**	IRF7779L2TRPBF	3
	Output	IPW65R035CFD7A	1

Table III: Component Selection (Magnetic Components)

	Magnetic Components		25 kHz	50 kHz	75 kHz	100 kHz
IPOP	**L1, L2, L3**	**Material**	MPP	High Flux	High Flux	Kool Mu HF
		Core	TVH61134A	0058091A2	C058076A2	0076071A7
CB	**L1**	**Material**	High Flux	High Flux	High Flux	High Flux
		Core	C058076A2	C058076A2	C058076A2	C058076A2
	L2	**Material**	High Flux	MPP	Kool Mu Max	Kool Mu Max
		Core	0058072A2	0055777A2	0079074A7	0079716A7
CF-PS-FB	**L_{Lk}**	**Material**	MPP	High Flux	High Flux	Kool Mu Max
		Core	C055438A2	C058071A2	C058584A2	0079894A7
	T1		Planar Transformer: HI-MAG 540			
DAB	**L_{Lk}**	**Material**	3C81	3C81	3C92	3C95
		Core	T140	T87	E65	ETD49
	T1		Planar transformer: HI-MAG 540			

Volume

The results from the volume analysis are shown in Table IV, where the volume is estimated in function of the switching frequency. The volume is reduced as the switching frequency increases, due to the reduction in size of the magnetic elements. The DAB presents the lowest volume throughout the evaluated switching frequency range. It is important to note that, although all four topologies comply with the maximum volume requirement of 4.6 dm^3, it is also important to evaluate the longitudinal measurement requirements. Fig. 8 shows a graphical representation of the maximum size of the converter and the magnetic elements, to evaluate the compliance with the dimension requirements. Only two topologies at two different frequencies are presented in Fig. 8, showing the front, top, and side views, where the converter's maximum dimensions (575x100x80 mm) are represented by a black rectangle, while the inductors and the transformers are shown in colors blue and cyan, respectively. For the inductor, the toroids are piled horizontally. The IPOP converter at 25 and at 75 kHz frequencies is shown in Fig. 8(a) and Fig. 8(c), respectively, where the 3 inductors overlap with the maximum length at 25 kHz but complies with requirements at 75 kHz. It can be appreciated that the DAB converter complies with the dimension requirements at both 25 and at 75 kHz, as it is appreciated in Fig. 8(b) and Fig. 8(c), respectively. The results of the volume analysis, which are not shown completely in this paper, conclude that the CF-PS-FB and the DAB comply throughout the whole frequency range, while the IPOP and the CB only fails to comply at 25 kHz, where they present the best efficiency results.

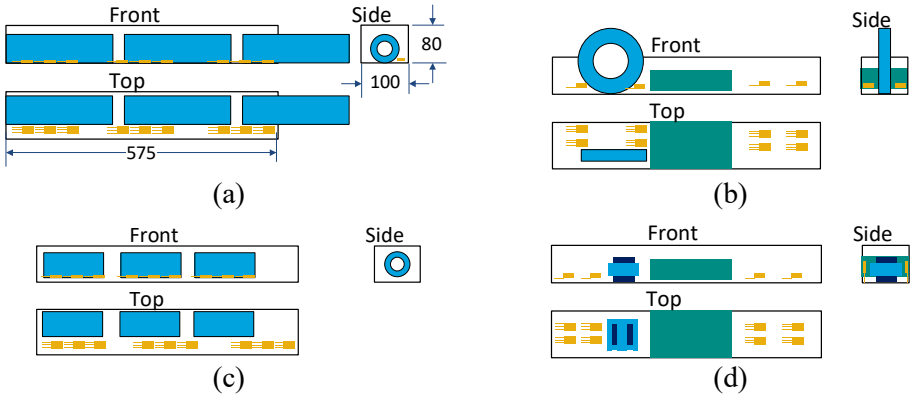

Fig. 8: Graphical representation of the converter maximum dimensions and the magnetic components. All the dimensions are in mm. (a) IPOP at 25 kHz. (b) DAB at 25 kHz. (c) IPOP at 75 kHz. (d) DAB at 75 kHz.

Table IV: Volume Estimation

Volumen [dm3]	**25 kHz**	**50 kHz**	**75 kHz**	**100 kHz**
IPOP	2.43	1.6	1.2	1.08
CB	3	2.96	2.17	1.23
CF-PS-FB	1.41	1	0.99	0.95
DAB	0.95	0.95	0.88	0.85

Conclusions

The IPOP and CB topologies present good efficiency results at low switching frequency, and also present the lowest input current ripple, due to their modular arrangement and interleaved control. However, at low frequencies, their length does not comply with the requirements, due to the number of inductors and their dimensions.

The CF-PS-FB and DAB, on the other hand, are able to operate under soft switching conditions, which allows them to increase the switching frequency without penalizing their efficiency. It is important to note that their dimensions comply with the requirements throughout all the frequency range.

The results show that the most adequate topology for this application is the DAB converter, as it presents the highest efficiency and power density throughout all the frequency range. Its main disadvantage is the high current ripple on both, the input and output. This implies the need of including filters, which will negatively affect its weight and volume. The CF-PS-FB is also an option, as its efficiency is around 1% less than the DAB and has a balanced current ripple at both ports. Both topologies have galvanic isolation, and even though is not a requirement, it benefits this application for safety reasons and because it allows to boost the voltage in a natural way.

As a result of this study, a prototype of the DAB converter, designed to operate at 75 kHz, is being built for testing the integration of removable batteries, where the future work will be focused on possible variations of the topology, control techniques, using wide-bandgap materials for 800 V HV-DC bus, among others.

References

[1] F. Blaabjerg, H. Wang, I. Vernica, B. Liu, and P. Davari, “Reliability of Power Electronic Systems for EV/HEV Applications,” *Proc. IEEE*, pp. 1–17, 2020.

[2] D. Dell'Isola, M. Urbain, M. Weber, S. Pierfederici, and F. Meibody-Tabar, "Optimal Design of a DC-DC Boost Converter in Load Transient Conditions, Including Control Strategy and Stability Constraint," *IEEE Trans. Transp. Electrif.*, vol. 5, no. 4, pp. 1214–1224, 2019.

[3] European Commission, "Paris Agreement | Climate Action." [Online]. Available: https://ec.europa.eu/clima/policies/international/negotiations/paris_en. [Accessed: 17-Jan-2022].

[4] H. Ko, S. Pack, and V. C. M. Leung, "An Optimal Battery Charging Algorithm in Electric Vehicle-Assisted Battery Swapping Environments," *IEEE Trans. Intell. Transp. Syst.*, pp. 1–10, 2020.

[5] Y. Song, J. Li, G. Ji, and Z. Xue, "Study on the typical mode of EV charging and battery swap infrastructure interconnecting to power grid," *China Int. Conf. Electr. Distrib. CICED*, vol. 2016-Septe, no. Ciced, pp. 10–13, 2016.

[6] R. P. Twiname, D. J. Thrimawithana, U. K. Madawala, and C. A. Baguley, "A Dual-Active Bridge Topology with a Tuned CLC Network," *IEEE Trans. Power Electron.*, vol. 30, no. 12, pp. 6543–6550, 2015.

[7] Z. Xian and G. Wang, "Optimal dispatch of electric vehicle batteries between battery swapping stations and charging stations," *IEEE Power Energy Soc. Gen. Meet.*, vol. 2016-Novem, 2016.

[8] Y. Zheng, Z. Y. Dong, Y. Xu, K. Meng, J. H. Zhao, and J. Qiu, "Electric vehicle battery charging/swap stations in distribution systems: Comparison study and optimal planning," *IEEE Trans. Power Syst.*, vol. 29, no. 1, pp. 221–229, Jan. 2014.

[9] M. A. H. Rafi, R. Rennie, J. Larsen, and J. Bauman, "Investigation of fast charging and battery swapping options for electric haul trucks in underground mines," in *2020 IEEE Transportation Electrification Conference and Expo, ITEC 2020*, 2020, pp. 1081–1087.

[10] Z. Chen, "The combination of battery swapping system and connected vehicles technology in intelligent transportation," *Proc. - 2020 Int. Conf. Intell. Transp. Big Data Smart City, ICITBS 2020*, pp. 72–75, 2020.

[11] S. Chowdhury, M. N. Bin Shaheed, and Y. Sozer, "State-of-Charge Balancing Control for Modular Battery System with Output DC Bus Regulation," *IEEE Trans. Transp. Electrif.*, vol. 7, no. 4, pp. 2181–2193, Dec. 2021.

[12] J. Reimers, L. Dorn-Gomba, C. Mak, and A. Emadi, "Automotive Traction Inverters: Current Status and Future Trends," *IEEE Trans. Veh. Technol.*, vol. 68, no. 4, pp. 3337–3350, Apr. 2019.

[13] O. C. Onar, J. Kobayashi, and A. Khaligh, "A Fully Directional Universal Power Electronic Interface for EV, HEV, and PHEV Applications," *Ieee Trans. Power Electron.*, vol. 28, no. 12, pp. 5489–5498, 2013.

[14] A. Vazquez, A. Rodriguez, D. G. Lamar, and M. M. Hernando, "Advanced Control Techniques to Improve the Efficiency of IPOP Modular QSW-ZVS Converters," *IEEE Trans. Power Electron.*, vol. 33, no. 1, pp. 73–86, 2018.

[15] F. H. Makarim, B. Antares, A. Rizqiawan, and P. A. Dahono, "Optimization of Multiphase Cascaded DC-DC Boost Converters," *ICEVT 2019 - Proceeding 6th Int. Conf. Electr. Veh. Technol. 2019*, pp. 285–289, 2019.

[16] R. S and S. Chellappan, "2-kW , 48- to 400-V , > 93 % Efficiency , Isolated Bidirectional DC-DC Converter Reference Design for UPS," no. June, pp. 1–30, 2017.

[17] K. Wang, C. Y. Lin, L. Zhu, D. Qu, F. C. Lee, and J. S. Lai, "Bi-directional dc to dc converters for fuel cell systems," *IEEE Work. Power Electron. Transp.*, vol. 11, pp. 47–51, 1998.

[18] S. Chi, P. Liu, X. Li, M. Xu, and S. Li, "A Novel Dual Phase Shift Modulation for Dual-Active- Bridge Converter," *2019 IEEE Energy Convers. Congr. Expo. ECCE 2019*, pp. 1556–1561, 2019.

[19] B. Zhao, Q. Song, and W. Liu, "Power characterization of isolated bidirectional dual-active-bridge dc-dc converter with dual-phase-shift control," *IEEE Trans. Power Electron.*, vol. 27, no. 9, pp. 4172–4176, 2012.

[20] C. D. A. Bridge, S. Bal, S. Member, D. B. Yelaverthi, and S. Member, "Improved Modulation Strategy Using Dual Phase Shift Modulation for Active Commutated," *IEEE Trans. Power Electron.*, vol. 33, no. 9, pp. 7359–7375, 2018.

[21] K. Martín Diaz, "Análisis , diseño y construcción de un proveedor de bus para sistemas de distribución en corriente continua domésticos," Universidad de Oviedo, 2018.

[22] Y. H. Abraham, H. Wen, W. Xiao, and V. Khadkikar, "Estimating power losses in Dual Active Bridge DC-DC converter," *2011 2nd Int. Conf. Electr. Power Energy Convers. Syst. EPECS 2011*, pp. 4–8, 2011.